23

Maximizing the sensitivity of thin film metal dielectric refractometers

© A.B. Sotsky[1], D.V. Ponkratov[1], E.A. Chudakov[1], L.I. Sotskaya[2]

[1] Mogilev State A. Kuleshov University,
Mogilev, Belarus
[2] Belarusian Russian University,
Mogilev, Belarus

e-mail: ab_sotsky@mail.ru

Received November 18, 2024
Revised April 16, 2025
Accepted July 03, 2025

A technique has been developed for calculating the reflectance of refractometers with a thin-film metal dielectric structure on the basis of a coupling prism, using multiplication of the characteristic matrices of the films. The characteristic matrices of the metallic films are obtained by numerical solution of the integral equations of the anomalous skin effect. Spectroscopic refractometers with the structure coupling-prism – gold film – dielectric film – water with a controllable refractive index were investigated. Fused quartz was chosen as the material for both the coupling prism and the dielectric film. The dielectric permittivity of the ionic lattice of gold and the constants of the electron gas in the gold films were determined from literature data on the spectral ellipsometry of gold films. It was shown that by choosing the thicknesses of the metallic and dielectric films, as well as the angle of incidence, one can combine two factors that lead to maximization of refractometer sensitivity — zero reflection from the base of the coupling prism and excitation in the dielectric film of a waveguide mode operating under conditions close to critical. When using s-polarized waves this allows the refractometer sensitivity to be increased to $9.6 \cdot 10^5$ nm/RIU. Estimates of the resolving power of thin-film metal dielectric refractometers based on the least-squares method are presented.

Keywords: optical sensor, thin film refractometer, anomalous skin effect, zero reflection, mode near critical conditions.

DOI: 10.61011/EOS.2025.08.62028.7357-25

1. Introduction

Thin-film refractometers are being investigated in connection with the development of highly sensitive compact sensors for chemical and biological components in solutions [1–7]. Refractometers of the spectroscopic type, in which an increment in the refractive index of the surrounding medium dn_s causes a shift of the minimum position $d\lambda$ of the position of the minimum in the device's reflection spectrum on the wavelength scale, are considered promising [1–3]. Such refractometers are characterized by a sensitivity factor $S = d\lambda/dn_s$ [1–3,8]. The most extensively studied refractometers are those that use resonance excitation of plasmon modes [1–8]. In particular, a three-layer metal-dielectric thin-film structure based on a coupling prism that guides a long-range plasmonic mode has made it possible to achieve, to date, a record sensitivity value of $S = 5.7 \cdot 10^4$ nm/RIU [1,3].

In the present paper we investigate the principal possibilities for further increasing the sensitivity of planar thin-film refractometers, i.e., maximizing $|S|$. The key idea is the simultaneous use of two factors that enhance the sensitivity of thin-film sensors: zero light reflection when exciting lossless Zenneck modes in the sensor structure [9,10] and operation of the coupling prism device near critical conditions [11]. Refractometers with the configuration coupling prism–gold film–dielectric film–water with controlled refractive index are considered. Fused quartz was chosen as the material for the coupling prism and dielectric film. The structure is excited by a plane wave of p or s polarization incident from the coupling prism side The spectrum of the energy reflection coefficient of light is analyzed. At the chosen wavelength, the angle of incidence and the film thicknesses are selected under conditions of zero reflection combined with excitation in the quartz film of a waveguide mode close to critical conditions. This allows raising the refractometer sensitivity up to $S = 9.7 \cdot 10^5$ nm/RIU. A criterion for evaluating the resolution capability of the considered refractometers, based on the least squares method, is proposed. The resolution capabilities of refractometers operating on p and s-polarization waves are compared. Calculations are performed based on model of the anomalous skin effect in metallic films. The dielectric permittivity of the ionic lattice and the constants of the electron gas in the gold films were determined by processing of literature data on spectral ellipsometry of nanoscale gold films.

2. Calculation method

The optical scheme of thin-film refractometers is shown in Fig. 1.

In region $y > 0$, there is a coupling prism with dielectric permittivity ε_a. On the base of the prism, a metal-

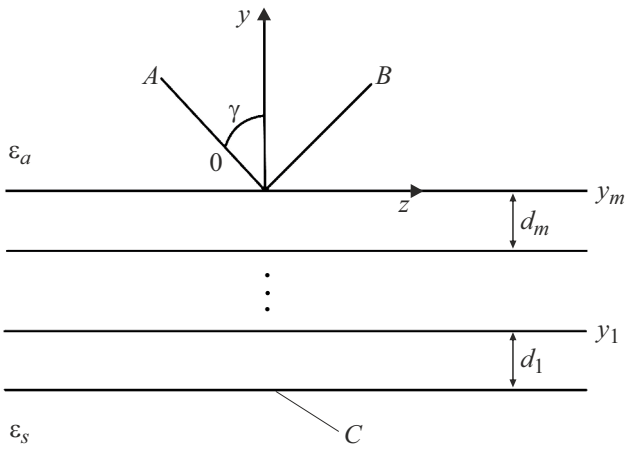

Figure 1. Optical scheme of thin-film refractometers.

dielectric structure consisting of m alternating metallic and dielectric films is applied. The thickness of the l-th film equals d_l, and the coordinate of its upper boundary is $y = y_l$. The relative dielectric permittivity of the dielectric films is ε_d. In the region $y < y_1 - d_1$ there is a dielectric medium with a measured refractive index n_s and dielectric permittivity $\varepsilon_s = (n_s - ik_s)^2$ (k_s is the absorption coefficient). A monochromatic plane wave depending on time t and coordinate z of the form $\exp(i\omega t - ik_0\beta z)$ (this factor will be omitted later) is incident on the structure from the $y > 0$ region at an angle γ. Here, $\beta = n_a \sin\gamma$, $n_a = \sqrt{\varepsilon_a}$, $k_0 = \omega/c = 2\pi/\lambda$ are wave numbers in vacuum. The homogeneity axis is Ox. A, B and C denote the amplitudes of the incident, reflected from the refractometer, and transmitted waves, respectively.

In the optics of metallic films, a widespread approach characterizes metals by a complex dielectric permittivity ε_n based on the Drude model of the normal skin effect [1–8,11–14]. The key element of this model is the assumption of a spatially local proportional relationship between the current density **j** and the electric field intensity **E** in the metal [15]. However, the metallic films in the refractometer structure are partially transparent to light. As a result, their thicknesses are comparable to the mean free path of conduction electrons in the metal [12,16]. Under such conditions, the assumption of a local connection between the **E** and **j** vectors in films, and therefore the applicability of the normal skin effect model to the calculation of these vectors, appears problematic. This problem can be associated with the observed thickness-dependent spectral data $\varepsilon_n(\lambda)$ in spectral ellipsometry of gold films [13,14]. A more accurate description of the electromagnetic field distribution in nanoscale metallic films can be obtained within the anomalous skin effect model, taking into account the spatially nonlocal relation between vectors **E** and **j** [16,17]. Below, this model is applied to the construction of characteristic matrices of metallic films and to the calculation of refractometers.

Let us first analyze the case of using s-polarized waves in the refractometer. For these waves, amplitudes A, B and C correspond to the electric field component E_x:

$$E_x(y) = A\exp(ik_{ya}k_0 y) + B\exp(-ik_{ya}k_0 y) \text{ at } y > y_m = 0, \quad (1)$$

$$E_x(y) = C\exp[ik_{ys}k_0(y - y_1 + d_1)] \text{ at } y < y_1 - d_1, \quad (2)$$

where $k_{ya,s} = \sqrt{\varepsilon_{a,s} - \beta^2}$.

Let us single out the film with number l in the structure. If the film is metallic, then according to [17],

$$E_x(\eta) = aE_x^{(1)}(\eta) + bE_x^{(2)}(\eta). \quad (3)$$

Here, a and b are certain constants, $\eta = y - y_l$, functions $E_x^{(1),(2)}(\eta)$ are solutions to Fredholm integral equations of the second kind:

$$E_x^{(j)}(\eta) = (2-j)\exp(ik_y k_0\eta) - (1-j)\exp(-ik_y k_0\eta)$$
$$- iK\varepsilon_n\pi \int_0^{\pi/2} d\theta \frac{\sin^3\theta}{(\alpha^2 + k_y^2)\cos\theta} \int_{-d_l}^{0} [\exp(-\alpha k_0|\eta - \eta'|)$$
$$+ Q_1(\eta,\eta') + Q_2(\eta,\eta')]E_x^{(j)}(\eta')d\eta', \quad (4)$$

where

$$j = 1, 2, \quad \eta = y - y_l, \quad k_y = \sqrt{\varepsilon_n - \beta^2},$$
$$K = -2e^2m^2v^2(\omega h^3\varepsilon_0\varepsilon_n)^{-1},$$
$$\alpha = (i\omega\tau + 1)(\omega\tau v c^{-1}\cos\theta)^{-1},$$
$$\varepsilon_n = \varepsilon + \Delta\varepsilon, \quad (5)$$

$$\Delta\varepsilon = \frac{2\pi i K\varepsilon_n}{k_0} \int_0^{\pi/2} \frac{\alpha\sin^3\theta}{(\alpha^2 + k_y^2)\cos\theta} d\theta, \quad (6)$$

$$Q_1(\eta,\eta') = \{\bar{p}_1\exp[-\alpha k_0(\eta + \eta')]$$
$$+ p_2\exp[\alpha k_0(\eta + \eta')]\}(1 - \bar{p}_1 p_2)^{-1},$$
$$Q_2(\eta,\eta') = 2\bar{p}_1 p_2\,\mathrm{ch}[\alpha k_0(\eta - \eta')](1 - \bar{p}_1 p_2)^{-1},$$
$$\bar{p}_1 = p_1\exp(-2\alpha k_0 d_l), \quad v = hm^{-1}\sqrt[3]{3n_0(8\pi)^{-1}},$$

ε is the dielectric permittivity of the ionic lattice of the metal, e is the electron charge, m is the electron mass, n_0 is the concentration of conduction electrons in the film material, p_1 and p_2 are probabilities of specular electron reflection from film boundaries $y = y_l - d_l$ and $y = y_l$, respectively, τ is the relaxation time or electron mean free path, h is Planck's constant, ε_0 is the vacuum dielectric permittivity.

The considered s-waves at the film boundaries have tangential components of the electromagnetic field E_x and $H_z = -i\omega\varepsilon_0 k_0^{-1}E_x'$, where $E_x' = k_0^{-1}\partial E_x/\partial\eta$. According to (4),

$$E_x'(\eta) = aE_x^{(1)'}(\eta) + bE_x^{(2)'}(\eta), \quad (7)$$

$$E_x^{(j)'}(\eta) = ik_y[(2-j)\exp(ik_yk_0\eta) + (1-j)\exp(-ik_yk_0\eta)]$$
$$- iK\varepsilon_n\pi\int_0^{\pi/2}\frac{d\theta\alpha\sin^3\theta}{(\alpha^2+k_y^2)\cos\theta}\int_{-d_l}^{0}[Q_4(\eta,\eta') - Q_3(\eta,\eta')$$
$$- \operatorname{sign}(\eta-\eta')\exp(-\alpha k_0|\eta-\eta'|)]E_x^{(j)}(\eta')d\eta', \quad (8)$$
$$Q_3(\eta,\eta') = \{\bar{p}_1\exp[(-\alpha k_0(\eta+\eta'))] - p_2\exp[\alpha k_0(\eta+\eta')]\}(1-\bar{p}_1p_2)^{-1},$$
$$Q_4(\eta,\eta') = 2\bar{p}_1p_2\,\mathrm{sh}[\alpha k_0(\eta-\eta')](1-\bar{p}_1p_2)^{-1},$$

where $j = 1, 2$. Alternately assuming in (3) and (7) $\eta = 0$, $\eta = -d_l$ and eliminating a and b from the resulting equations, we find

$$\mathbf{X}_{l+1}^{(s)} = \mathbf{M}_l^{(s)}\mathbf{X}_l^{(s)}. \quad (9)$$

where $\mathbf{X}_l^{(s)}$, $\mathbf{X}_{l+1}^{(s)}$ are column vectors with components

$$(\mathbf{X}_l^{(s)})_1 = E_x(-d_l), \quad (\mathbf{X}_l^{(s)})_2 = E_x'(-d_l),$$
$$(\mathbf{X}_{l+1}^{(s)})_1 = E_x(0), \quad (\mathbf{X}_{l+1}^{(s)})_2 = E_x'(0), \quad (10)$$

$\mathbf{M}_l^{(s)}$ — is the matrix 2×2 with elements

$$(\mathbf{M}_l^{(s)})_{11} = \Delta_s^{-1}[E_x^{(1)'}(-d_l)E_x^{(2)}(0) - E_x^{(2)'}(-d_l)E_x^{(1)}(0)], \quad (11)$$
$$(\mathbf{M}_l^{(s)})_{12} = \Delta_s^{-1}[E_x^{(2)}(-d_l)E_x^{(1)}(0) - E_x^{(1)}(-d_l)E_x^{(2)}(0)], \quad (12)$$
$$(\mathbf{M}_l^{(s)})_{21} = \Delta_s^{-1}[E_x^{(1)'}(-d_l)E_x^{(2)'}(0) - E_x^{(1)'}(0)E_x^{(2)'}(-d_l)], \quad (13)$$
$$(\mathbf{M}_l^{(s)})_{22} = \Delta_s^{-1}[E_x^{(1)'}(0)E_x^{(2)}(-d_l) - E_x^{(2)'}(0)E_x^{(1)}(-d_l)], \quad (14)$$

where

$$\Delta_s = E_x^{(2)}(-d_l)E_x^{(1)'}(-d_l) - E_x^{(1)}(-d_l)E_x^{(2)'}(-d_l).$$

Functions $E_x^{(1)}(\eta)$, $E_x^{(2)}(\eta)$, $E_x^{(1)'}(\eta)$, $E_x^{(2)'}(\eta)$, and hence matrix $\mathbf{M}_l^{(s)}$ allow numerical calculation by the quadrature method, the scheme of which is presented in [16].

If the number l corresponds to a dielectric film, then relations (7)–(14) remain valid. However, since $n_0 = 0$, we have $\varepsilon_n = \varepsilon_d$, $\Delta\varepsilon = 0$. The integral parts in (4) and (8) vanish. As a result, matrix $\mathbf{M}_l^{(s)}$ is found analytically:

$$(\mathbf{M}_l^{(s)})_{11} = (\mathbf{M}_l^{(s)})_{22} = \cos(\sigma k_0 d_l),$$
$$(\mathbf{M}_l^{(s)})_{12} = \sigma^{-1}\sin(\sigma k_0 d_l), \quad (\mathbf{M}_l^{(s)})_{21} = -\sigma\sin(\sigma k_0 d_l), \quad (15)$$

where $\sigma = \sqrt{\varepsilon_d - \beta^2}$.

Taking into account (1), (2) and the continuity conditions of tangential components of the electromagnetic field at film boundaries for the amplitude reflection coefficient of the s-wave from the refractometer, we have

$$r_s = \frac{B}{A} = \frac{ik_{ya}L_{11}^{(s)} - L_{21}^{(s)} + ik_{ys}(ik_{ya}L_{12}^{(s)} - L_{22}^{(s)})}{ik_{ya}L_{11}^{(s)} + L_{21}^{(s)} + ik_{ys}(ik_{ya}L_{12}^{(s)} + L_{22}^{(s)})}, \quad (16)$$

where

$$\mathbf{L}^{(s)} = \mathbf{M}_m^{(s)}\mathbf{M}_{m-1}^{(s)}\ldots\mathbf{M}_1^{(s)}. \quad (17)$$

For p-polarized waves, the nonzero electromagnetic field components are H_s, E_y, E_z. Amplitudes A, B and C correspond to the magnetic field component H_x:

$$H_x = A\exp(ik_{ya}k_0y) + B\exp(-ik_{ya}k_0y) \text{ at } y > 0,$$
$$H_x = C\exp[ik_{ys}k_0(y - y_1 + d_1)] \text{ at } y < y_1 - d_1.$$

Let the number l correspond to a metallic film. In it, E_y and E_z are represented as sums [17]

$$E_y(\eta) = aE_y^{(1)}(\eta) + bE_y^{(2)}(\eta), \quad E_z(\eta) = aE_z^{(1)}(\eta) + bE_z^{(2)}(\eta),$$

where a and b are certain constants, and functions $E_y^{(j)}(\eta)$, $E_z^{(j)}(\eta)$ satisfy the system of two Fredholm integral equations of the second kind

$$E_z^{(j)}(\eta) = (2-j)\exp(ik_yk_0\eta) - (1-j)\exp(-ik_yk_0\eta)$$
$$- K\pi\int_0^{\pi/2}d\theta\frac{\sin\theta}{\alpha^2+k_y^2}\int_{-d_l}^{0}\left\{\frac{ik_y^2\sin^2\theta}{\cos\theta}E_z^{(j)}(\eta')\right.$$
$$\times\left[\exp(-\alpha k_0|\eta-\eta'|) + Q_1(\eta,\eta') + Q_2(\eta,\eta')\right]$$
$$\left. - 2\alpha\beta\cos\theta E_y^{(j)}(\eta')\left[\operatorname{sign}(\eta-\eta')\exp(-\alpha k_0|\eta-\eta'|)\right.\right.$$
$$\left.\left. - Q_3(\eta,\eta') - Q_4(\eta,\eta')\right]\right\}d\eta', \quad (18)$$
$$E_y^{(j)}(\eta) = \frac{\beta}{k_y}[(2-j)\exp(ik_yk_0\eta) + (1-j)\exp(-ik_yk_0\eta)]$$
$$+ iK\pi\int_0^{\pi/2}d\theta\frac{\sin\theta}{\alpha^2+k_y^2}\int_{-d_l}^{0}\left\{\frac{i\alpha\beta\sin^2\theta}{\cos\theta}E_z^{(j)}(\eta')\right.$$
$$\times\left[Q_4(\eta,\eta') - Q_3(\eta,\eta') - \operatorname{sign}(\eta-\eta')\exp(-\alpha k_0|\eta-\eta'|)\right]$$
$$+ 2(\alpha^2+\varepsilon_n)\cos\theta E_y^{(j)}(\eta')\left[Q_1(\eta,\eta') - Q_2(\eta,\eta')\right.$$
$$\left.\left. - \exp(-\alpha k_0|\eta-\eta'|)\right]\right\}d\eta' + \frac{\Delta\varepsilon}{\varepsilon_n}E_y(\eta), \quad (19)$$

where $j = 1, 2$. According to Maxwell's equations and equations (18), (19),

$$H_x(\eta) = i\omega\varepsilon_0k_0^{-1}H(\eta),$$

where

$$H(\eta) = k_0^{-1}[\partial E_z/\partial\eta + i\beta k_0E_y(\eta)] = aH_1(\eta) + bH_2(\eta),$$

$$H_j(\eta) = \frac{i\varepsilon_n}{k_y}\left[(2-j)\exp(ik_yk_0\eta) - (j-1)\exp(-ik_yk_0\eta)\right]$$

$$- i\pi\varepsilon_n K\int_0^{\pi/2} d\theta\,\frac{\sin\theta}{\alpha^2+k_y^2}\int_{-d_l}^{0}\left\{\frac{\alpha\sin^2\theta}{\cos\theta}E_z(\eta')\right.$$

$$\times\left[Q_4(\eta,\eta') - Q_3(\eta,\eta') - \mathrm{sign}(\eta-\eta')\exp\left(-\alpha k_0|\eta-\eta'|\right)\right]$$

$$- 2i\beta\cos\theta\,E_y(\eta')\left[Q_1(\eta,\eta') - Q_2(\eta,\eta')\right.$$

$$\left.\left. - \exp\left(-\alpha k_0|\eta-\eta'|\right)\right]\right\}d\eta'.$$

Numerical solution of systems (18), (19) with subsequent calculation of functions $H_j(\eta)$ can be performed by the quadrature method [16,17]. For p-waves, relations analogous to (9)–(14), have the form

$$\mathbf{X}_{l+1}^{(p)} = \mathbf{M}_l^{(p)}\mathbf{X}_l^{(p)},$$

$$(\mathbf{X}_l^{(p)})_1 = H(-d_l), \quad (\mathbf{X}_l^{(p)})_2 = E_z(-d_l),$$

$$(\mathbf{X}_{l+1}^{(p)})_1 = H(0), \quad (\mathbf{X}_{l+1}^{(p)})_2 = E_z(0),$$

$$(\mathbf{M}_l^{(p)})_{11} = \Delta_p^{-1}\left[H_2(0)E_z^{(1)}(-d_l) - H_1(0)E_z^{(2)}(-d_l)\right],$$

$$(\mathbf{M}_l^{(p)})_{12} = \Delta_p^{-1}\left[H_1(0)H_2(-d_l) - H_1(-d_l)H_2(0)\right],$$

$$(\mathbf{M}_l^{(p)})_{21} = \Delta_p^{-1}\left[E_z^{(2)}(0)E_z^{(1)}(-d_l) - E_z^{(1)}(0)E_z^{(2)}(-d_l)\right],$$

$$(\mathbf{M}_l^{(p)})_{22} = \Delta_p^{-1}\left[H_2(-d_l)E_z^{(1)}(0) - H_1(-d_l)E_z^{(2)}(0)\right],$$

where

$$\Delta_p = H_2(-d_l)E_z^{(1)}(-d_l) - H_1(-d_l)E_z^{(2)}(-d_l).$$

For dielectric films,

$$(\mathbf{M}_l^{(p)})_{11} = (\mathbf{M}_l^{(p)})_{22} = \cos(\sigma k_0 d_l),$$

$$(\mathbf{M}_l^{(p)})_{12} = -\frac{\varepsilon_d\sin(\sigma k_0 d_l)}{\sigma},\ (\mathbf{M}_l^{(p)})_{21} = \frac{\sigma\sin(\sigma k_0 d_l)}{\varepsilon_d}. \tag{20}$$

Analogs of expressions (16), (17) are

$$r_p = \frac{B}{A} = \frac{L_{12}^{(p)}ik_{ya}\varepsilon_a^{-1} + L_{22}^{(p)} - L_{11}^{(p)}\varepsilon_s k_{ya}\varepsilon_a^{-1}k_{ys}^{-1} + L_{21}^{(p)}i\varepsilon_s k_{ys}^{-1}}{L_{12}^{(p)}ik_{ya}\varepsilon_a^{-1} - L_{22}^{(p)} - L_{11}^{(p)}\varepsilon_s k_{ya}\varepsilon_a^{-1}k_{ys}^{-1} - L_{21}^{(p)}i\varepsilon_s k_{ys}^{-1}}, \tag{21}$$

$$\mathbf{L}^{(p)} = \mathbf{M}_m^{(p)}\mathbf{M}_{m-1}^{(p)}\ldots\mathbf{M}_1^{(p)}.$$

It should be noted that the free terms of integral equations (4), (18), and (19) coincide with the components of the electromagnetic field found in the approximation of the normal skin effect. This approximation provides an exact description of the field inside the metallic film only in the limit $\omega\tau \to 0$, when the kernels of equations (4), (18), and (19) vanish [16], and the matrices $\mathbf{M}_l^{(s)(p)}$ have the analytical form (15), (20), where ε_d is replaced by ε_n. However, for nanoscale metallic films, the results of optical field and reflection coefficient calculations obtained within the normal and anomalous skin effect models can differ significantly [16,17].

Table 1. Electronic gas parameters in gold films of different thicknesses d_1

d_1, nm	τ, s	n_0, m^{-3}	p_1	p_2	a_1	a_2, nm^2
25	$0.90\cdot10^{-14}$	$5.81\cdot10^{28}$	0.01	0.47	3.53	$2.87\cdot10^{6}$
53	$1.12\cdot10^{-14}$	$5.86\cdot10^{28}$	1.00	0.55	3.56	$2.58\cdot10^{6}$
117	$1.31\cdot10^{-14}$	$5.69\cdot10^{28}$	1.00	0.69	3.62	$2.50\cdot10^{6}$

3. Parameters of Gold Films

Assigning parameters for metallic films is crucial for calculating the considered refractometers. The discussion below refers to gold films. The wide use of such films in photonics devices is due to their resistance to oxidation, thermal stability, and high conductivity.

In the anomalous skin effect model, a metallic film, in addition to its thickness, is characterized by the dielectric permittivity of the metal ionic lattice $\varepsilon(\lambda)$ and four electronic gas parameters n_0, τ, p_1, p_2 (see the previous section). Since the integral parts of equations (4), (18), and (19) are significant for nanoscale metallic films [16,17], the function $\varepsilon_n(\lambda)$ does not have an independent meaning.

To determine the parameters of gold films, we used experimental data from [14], where spectral ellipsometry of gold films deposited by electron-beam evaporation on a silicon substrate was performed. In [14] a table of $\varepsilon_n(\lambda)$ spectra in the range $300 \le \lambda \le 2000$ nm with 10 nm steps for three films with thicknesses 25, 53, and 117 nm, evaluated using X-ray structural analysis, is provided. These spectra were obtained based on the normal skin effect model by solving the inverse problem of spectral ellipsometry of metallic films of given thickness with known $\varepsilon_s(\lambda)$ dependence for the substrate. Under these conditions, spectral data $\delta_e(\lambda) = r_p(\lambda)/r_s(\lambda)$can be matched to experimental $\varepsilon_n(\lambda)$ data by calculating $r_p(\lambda)$ and $r_s(\lambda)$ in the normal skin effect approximation. On the other hand, theoretical function $\delta_i(\lambda) = r_p(\lambda)/r_s(\lambda)$can be found using formulas of the anomalous skin effect given in the previous section. Comparing dependencies $\delta_e(\lambda)$ and $\delta_i(\lambda)$ allows solving the inverse spectral ellipsometry problem of determining parameters$n$, τ, p_1, p_2, $\varepsilon(\lambda)$. Corresponding calculations were done at $\gamma = 70°$ [14], $m = 1$, $\varepsilon_a = 1.0003^2$ (the region $y > 0$ is occupied by air), and with $\varepsilon_s(\lambda)$ function set based on known data for refractive indices and absorption of silicon [18].

The inverse problem of spectral ellipsometry for gold films was solved in two steps. Initially, the spectral range $1000 \le \lambda \le 2000$ nm, was analyzed, where the experimental spectra of the complex dielectric permittivity of gold are monotonic [12–14]. For the function $\varepsilon(\lambda)$, a two-parameter Cauchy model was used:

$$\varepsilon(\lambda) = a_1 + a_2/\lambda^2$$

and six anomalous skin effect model parameters n_0, τ, p_1, p_2, a_1, a_2 were determined by minimizing the target function

$$F(n_0, \tau, p_1, p_2, a_1, a_2) = \sum_{j=1}^{101} \left| \delta_e(\lambda_j) - \delta_i(\lambda_j, n_0, \tau, p_1, p_2, a_1, a_2) \right|^2,$$

where $\lambda_1 = 1000$ nm, $\lambda_{101} = 2000$ nm. During calculations, values ε_n of type (5) were computed by numerical solution of the transcendental equation (6) with respect to $\Delta\varepsilon$ by the contour integration method [19]. The obtained results are shown in Table 1.

The observed increase in values τ, p_1, p_2 with increasing d_1 in Table 1 can be associated with an increase in the crystallinity degree of gold as the film grows [14].

At the second step, the found values n, τ, p_1, p_2 were fixed, and for all tabulated wavelengths in the full experimental range $300 \le \lambda \le 2000$ nm equation $\delta_e = \delta_i(\varepsilon)$ was solved with respect to ε for each of the three films using the contour integration method. The graphs of the obtained $\varepsilon(\lambda)$ functions and their corresponding $\varepsilon_n(\lambda)$ functions of type (5) are shown in Fig. 2 by solid lines. Dashed lines correspond to data from [14].

According to Fig. 2, unlike the $\varepsilon_n(\lambda)$ function, the spectrum of dielectric permittivity of the gold ionic lattice $\varepsilon(\lambda)$ is relatively stable with respect to film thickness. Some discrepancies in $\varepsilon(\lambda)$ distributions for the three films in Fig. 2 likely arise from experimental errors. Note also the mismatch of solid and dashed curves in Fig. 2, *b*, related to $d_1 = 25$ nm andFx163xE nm, which indicates the significant role of integral terms in equations (4), (18), and (19).

4. Refractometer Characteristics

Refractometers using a coupling prism made of fused quartz, whose dielectric permittivity $\varepsilon_a(\lambda)$ is given by a three-term Sellmeier formula [20], with the imaginary part of ε_a considered negligibly small, are studied. At the base of the coupling prism, there is either a single gold film ($d_1 = 0$, $d_2 \neq 0$) or a two-film metal-dielectric structure (Fig. 1). In the latter case, the gold film contacts the coupling prism, and the dielectric film material is quartz ($\varepsilon_1 = \varepsilon_a$). This configuration fundamentally differs from the known configuration for exciting long-range plasmon modes, where the dielectric film adjoins the coupling prism [1,3]. In region $y < y_1 - d_1$, water with refractive index and absorption coefficients n_s and k_s is located. The function $\varepsilon_s(\lambda) = [n_s(\lambda) - ik_s(\lambda)]^2$ for pure water is given by the dispersion table from [21]. Calculations were performed near the wavelength $\lambda_0 = 800$ nm, where $\varepsilon_a(\lambda_0) = 2.112205$, $n_s(\lambda_0) = 1.329$, $k_s(\lambda_0) = 1.25 \cdot 10^{-7}$, and the averaged $\varepsilon(\lambda)$ dependence over three films (Fig. 2) can be interpolated as

$$\varepsilon(\lambda) = 6.87 - i0.119 - (4.81 - i1.12) \cdot 10^{-3}(\lambda - \lambda_0).$$

For calculations, averaged values from Table 1, $\tau = 10^{-14}$ s, and $n_0 = 5.8 \cdot 10^{28}$ m^{-3} were chosen. To clarify the influence of gold film boundary smoothness on refractometer characteristics, two limiting cases with electron specular reflection probabilities $p_1 = p_2 = 0$ or $p_1 = p_2 = 1$ were considered.

Two types of refractometers were studied. The first type has the standard Kretschmann scheme with a single gold film and operates with *p*-polarized waves [1]. The second type has the above-described two-film structure. Waves of both *p* and *s*-polarization may be used in it.

The first step in optimizing refractometers is achieving zero light reflection from the coupling prism at the wavelength $\lambda = \lambda_0$ [9,10]. For the first type of refractometer, this means satisfying the conditions

$$\mathrm{Re}(r_p) = 0, \quad \mathrm{Im}(r_p) = 0, \tag{22}$$

which represent a system of two transcendental equations for the angle of incidence γ and gold film thickness d_2. For second-type refractometers, in addition to (22), the following conditions are also fulfilled

$$\mathrm{Re}(r_s) = 0, \quad \mathrm{Im}(r_s) = 0. \tag{23}$$

Calculations performed by the iteration method [22] showed that for second-type refractometers, equations (22) or (23) can be identically satisfied by properly choosing film thicknesses d_1 and d_2 at arbitrary incidence angle γ. Physically, this corresponds to reflectionless prism excitation of dielectric film modes through the metallic buffer layer. Fragments of dependence of roots of equations (22) and (23) on γnear the critical total internal reflection angle

$$\gamma_c = \arcsin\left(n_s / \sqrt{\varepsilon_a}\right), \tag{24}$$

corresponding to the excitation of fundamental modes, are shown in Fig. 3.

In Fig. 3, dependencies $d_1(\gamma)$ and $d_2(\gamma)$ related to *p*- and *s*-polarized waves differ significantly. These dependencies are influenced by electron specular reflection probabilities p_1, p_2. The case $\gamma \to \gamma_c$ corresponds to excitation of the fundamental mode of the dielectric film near critical conditions. This case is of primary interest for maximizing refractometer sensitivity.

Indeed, if the registered parameter upon variations of n_s is the shift $d\lambda$ of the minimum coordinate of functions $|r_p(\lambda)|^2$ or $|r_s(\lambda)|^2$ and at the initial value n_s conditions (22) or (23) are satisfied, then increments dn_s and $d\lambda$ are related by the relation

$$S_{p,s} = \frac{d\lambda}{dn_s} = \mathrm{Re}\left(\frac{\partial r^*_{p,s}}{\partial n_s} \frac{\partial r_{p,s}}{\partial \lambda} \right) \left| \frac{\partial r_{p,s}}{\partial \lambda} \right|^{-2}. \tag{25}$$

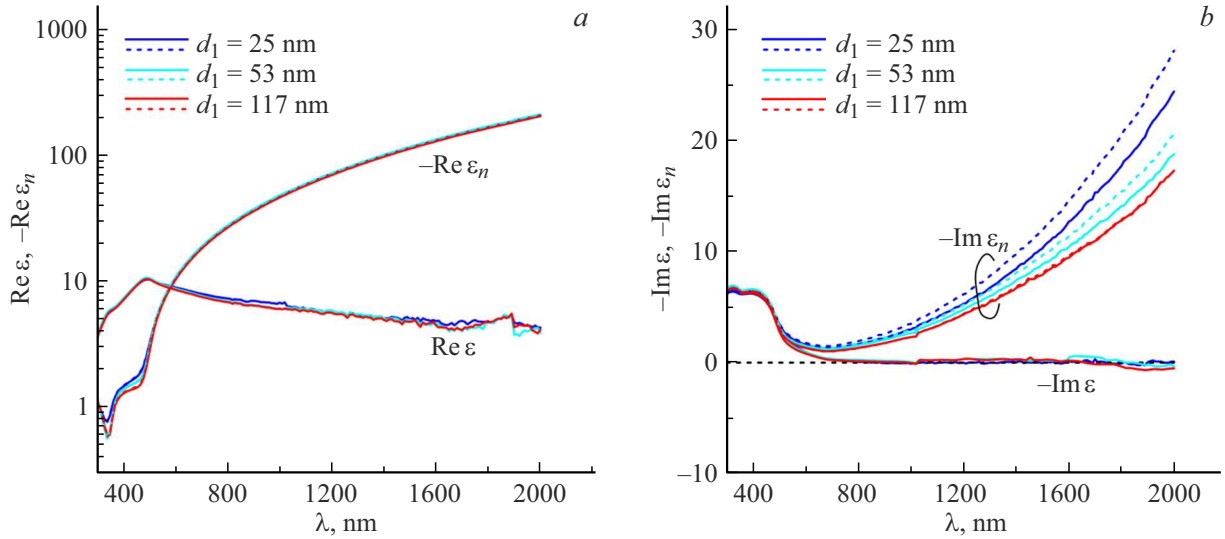

Figure 2. Spectra of the real (a) and imaginary (b) parts of dielectric permittivities ε and ε_n for gold films of different thicknesses. The horizontal dashed line indicates the zero level.

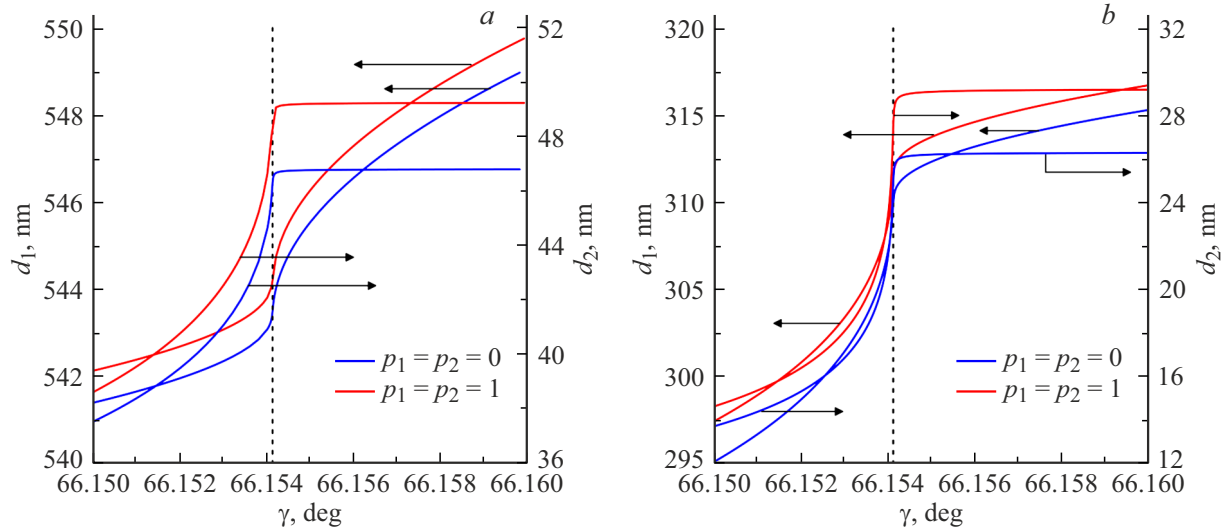

Figure 3. Thicknesses of quartz (d_1) and gold (d_2) films providing zero light reflection from the two-film refractometer as functions of the light incidence angle and electron specular reflection probabilities from gold film boundaries p_1, p_2: a — p-polarized waves, b — s-polarized waves. Dashed lines correspond to the critical angle (24).

Table 2. Parameters of first- and second-type thin-film refractometers when selecting film thicknesses from conditions (22), (23)

Mode	p_1	p_2	γ, deg	d_1, nm	d_2, nm	S_p, nm/RIU	S_s, nm/RIU	C	C'
p_0	0	0	71.326	0	47.56	7022	–	$9.41 \cdot 10^{-3}$	$9.96 \cdot 10^{-3}$
	1	1	71.264	0	50.00	7036	–	$6.24 \cdot 10^{-3}$	$6.59 \cdot 10^{-3}$
p_1	0	0	66.155	545.56	46.75	259407	–	$6.96 \cdot 10^{-5}$	$6.90 \cdot 10^{-5}$
	1	1	66.155	546.30	49.18	258516	–	$5.06 \cdot 10^{-5}$	$4.97 \cdot 10^{-5}$
s_1	0	0	66.155	312.35	26.21	–	956393	$2.93 \cdot 10^{-5}$	$2.96 \cdot 10^{-5}$
	1	1	66.155	313.76	29.09	–	966546	$2.05 \cdot 10^{-5}$	$2.06 \cdot 10^{-5}$

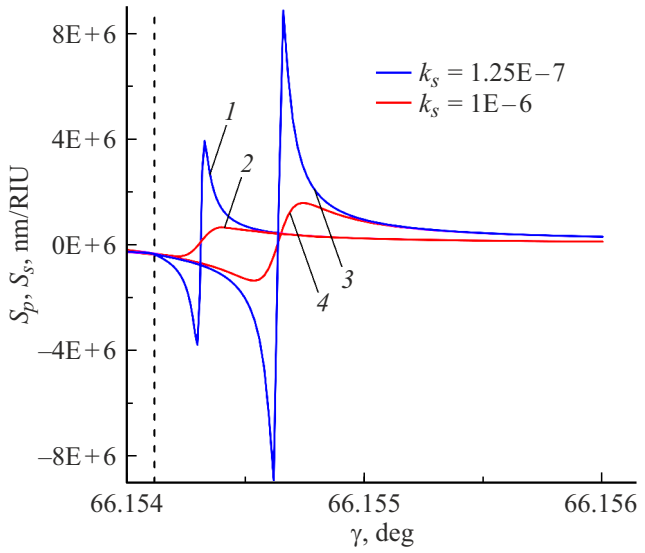

Figure 4. Sensitivity of two-film refractometers when using waves of *p*- (*1, 2*) and *s*- (*3, 4*) polarization. Dashed straight line indicates the critical angle (24).

where S_p and S_s are sensitivity factors of the refractometer when using waves of *p*- or *s*-polarization, with an asterisk denoting complex conjugation. According to (16) and (21),

$$\frac{\partial r_s}{\partial n_s}=\frac{2\sqrt{\varepsilon_s}\left(L_{12}^{(s)}L_{21}^{(s)}-L_{11}^{(s)}L_{22}^{(s)}\right)}{k_{ys}k_{ya}\left[L_{11}^{(s)}+L_{21}^{(s)}(ik_{ya})^{-1}+ik_{ys}\left(L_{12}^{(s)}+L_{22}^{(s)}(ik_{ya})^{-1}\right)\right]^2}, \tag{26}$$

$$\frac{\partial r_p}{\partial n_s}=\frac{2\varepsilon_a(k_{ys}^2-\beta^2)\left(L_{11}^{(p)}L_{22}^{(p)}-L_{12}^{(p)}L_{21}^{(p)}\right)}{k_{ys}k_{ya}\varepsilon_s^{3/2}\left\{L_{11}^{(p)}-L_{21}^{(p)}\varepsilon_a(ik_{ya})^{-1}+ik_{ys}\varepsilon_s^{-1}\left[L_{22}^{(p)}\varepsilon_a(ik_{ya})^{-1}-L_{12}^{(p)}\right]\right\}^2}. \tag{27}$$

At $\gamma\to\gamma_c$ we have $k_{ys}\to\sqrt{-k_s(k_s+2in_s)}$. From (25)–(27) it follows that in this limit, with weak light absorption in the investigated medium ($k_s\to 0$) large moduli $|S_{p,s}|$can be expected.

This conclusion is supported by the graphs shown in Fig. 4. They were constructed using formulas (25)–(27) with d_1 and d_2 chosen according to Fig. 3 data. Derivatives $\partial r_{p,s}/\partial\lambda$ were calculated numerically based on (16) and (21).

In Fig. 4, curves corresponding to cases $p_1=p_2=0$ and $p_1=p_2=1$coincide at the scale of the figure, but this coincidence occurs at different combinations of film thicknesses d_1 and d_2 (Fig. 3 and Table 2). It is seen that extreme sensitivities of refractometers are achieved at $\gamma\to\gamma_c$ from the side of incidence angles providing total internal reflection of light from the dielectric film–water interface. In accordance with (25)–(27) moduli $|S_{p,s}(\gamma)|$ sharply decrease with increasing k_s, and at $\gamma=\gamma_1=66.15435^\circ$ and $\gamma=\gamma_2=66.15463^\circ$ functions $S_p(\gamma)$ and $S_s(\gamma)$ change sign. In the region $\gamma>\gamma_2$, where $S_s(\gamma)>0$, $S_p(\gamma)>0$, the inequality $S_s(\gamma)>S_p(\gamma)$ holds, so the use of *s*-polarized waves is preferable. At $k_s=1.25\cdot10^{-7}$ a sharp maximum of function $S_s(\gamma)$ equal to $8.88\cdot10^6$ nm/RIU is achieved at $\gamma=66.15466^\circ$. However, such fine adjustment of the angle of incidence is technically difficult, so further characteristics of two-film refractometers are considered at $\gamma=66.155^\circ$where they are less sensitive to k_s (Fig. 4).

Calculations show that near the incidence angle $\gamma=\gamma_c$ the systems of equations (22) and (23) have many solutions differing mainly in d_1 values, separated by intervals $\Delta d_1=0.5\lambda_0/\sqrt{\varepsilon_a(\lambda_0)-n_s^2(\lambda_0)}$ characteristic of critical thicknesses of dielectric film modes of different orders [20]. However, higher modes are not of significant interest because their excitation produces $|S_{p,s}(\gamma)|$ moduli much smaller than those of fundamental modes.

These features are illustrated by Table 2. Its p_0 rows correspond to plasmon mode excitation in the Kretschmann scheme; rows p_1 and s_1 correspond to excitation of fundamental *p*- and *s*-polarized modes in the dielectric film of the refractometers.

According to Table 2, optimized two-film refractometers have much higher sensitivity compared to refractometers with the Kretschmann scheme. Table 2 also indicates that from the viewpoint of maximizing sensitivity, refractometers using *s*-polarization waves are preferable. The average sensitivity over two s_1 rows in Table 2 is $S_s=9.6\cdot10^5$ nm/RIU, which exceeds by more than an order of magnitude the record $5.7\cdot10^4$ nm/RIU, value achieved by excitation of long-range plasmon modes in [1].

The influence of the increment in water refractive index Δn_s on the reflection spectra of refractometers is illustrated in Fig. 5. The presented curves correspond to the data given in Table 2.

According to Fig. 5, the $|r_{p,s}(\lambda)|^2$ spectra differ significantly between diffuse ($p_1=p_2=0$) and specular ($p_1=p_2=1$) reflection of conduction electrons from the gold film boundaries. The presented graphs correlate with the sensitivities of the corresponding refractometers. In particular, at the scale of Fig. 5, *a*, curves related to $\Delta n_s=0$ (pure water) and $\Delta n_s\le5\cdot10^{-6}$ are visually indistinguishable. In Fig. 5, *b*, a similar situation occurs at $\Delta n_s\le1\cdot10^{-6}$.

Along with sensitivity, an important characteristic of refractometers is their resolution $r$understood as the smallest reliably detectable change in refractive index n_s. The value r is determined by the statistical properties of light, noise in the photodetector electronic circuitry, and rounding errors during analog-to-digital signal conversion [2].

As an estimate of r one can take the root mean square deviation of the measured value n_s [2,8]. Under prism excitation of plasmon modes, the reflection spectrum of the coupling prism $R(\lambda)=|r_p(\lambda)|^2$ has a single minimum at $\lambda=\lambda_{\min}$where the value $\lambda_{\min}$ is uniquely related to n_s [2]. Thus, to monitor n_s one can use dependence $n_s(\lambda_{\min})$. In this case, $r=\sigma_\lambda S^{-1}$, where σ_λ is the root mean square deviation of $\lambda_{\min}$ [2,8]. Estimates of values $\lambda_{\min}$ and σ_λ can be obtained by processing the data set $R_j=R(\lambda_j)$, measured at discrete wavelengths λ_j, using regression analysis or the centroid method [23]. However, such calculations require the minimum of function $R(\lambda)$ on some

interval $a \le \lambda \le b$ containing a sufficiently large number of N λ_j nodes to be unique, and increment Δn_s should cause a shift of the $R(\lambda)$ contour while preserving its shape (Fig. 5, *a*), which is typical for plasmon mode excitation.

For the considered two-film refractometers, these conditions are not fulfilled. Indeed, in Fig. 5, *b*, where $R(\lambda) = |r_p(\lambda)|^2$, and Fig. 5, *c*, where $R(\lambda) = |r_s(\lambda)|^2$, the $R(\lambda)$spectra related to $\Delta n_s = 0$ have two minima, one of which (zero) corresponds to excitation of the whole structure's Zenneck mode, and the other to the excitation of the fundamental dielectric film mode. Moreover, the modification of $R(\lambda)$ contours with increasing Δn_s looks more like narrowing than shifting.

In this situation, the least squares method can be used to control n_s where n_s is determined from the condition of minimum of the target function

$$F(n_s) = \sum_{j=1}^{N} [R_j - f_j(n_s)]^2, \tag{28}$$

where R_j are experimental data, $f_j(n_s)$ is the theoretical model of form (16) or (21) (more precisely, $f_j(n_s) = |r_s(\lambda_j, n_s)|^2$ or $f_j(n_s) = |r_p(\lambda_j, n_s)|^2$, depending on the radiation polarization). Denote by $\bar{R}_j$ the average of the random variable R_j (here and below a bar over the expression denotes averaging). Then, in the linear approximation justified for small $R_j$fluctuations, the function $f_j(n_s)$ in (28) can be taken in the form

$$f_j(n_s) = f_j(\bar{n}_s) + \left(\frac{\partial f_j}{\partial n_s}\right)_{n_s=\bar{n}_s} \Delta n_s, \tag{29}$$

where $\Delta n_s = n_s - \bar{n}_s$, $\bar{n}_s$ are roots of the equation

$$\sum_{j=1}^{N} [\bar{R}_j - f_j(n_s)] \frac{\partial f_j}{\partial n_s} = 0. \tag{30}$$

From the minimum condition of $F(n_s)$ with (29), we get

$$\Delta n_s = \sum_{j=1}^{N} \left\{ [R_j - f_j(\bar{n}_s)] \left(\frac{\partial f_j}{\partial n_s}\right)_{n_s=\bar{n}_s} \right\} \left[\sum_{j=1}^{N} \left(\frac{\partial f_j}{\partial n_s}\right)^2_{n_s=\bar{n}_s} \right]^{-1}. \tag{31}$$

According to (30) and (31), $\overline{\Delta n_s} = 0$. Then, assuming statistical independence of R_j values at different j are statistically independent,

$$r = \sqrt{\sum_{j=1}^{N} \left[D(R_j) \left(\frac{\partial f_j}{\partial n_s}\right)^2_{n_s=\bar{n}_s} \right]} \left[\sum_{j=1}^{N} \left(\frac{\partial f_j}{\partial n_s}\right)^2_{n_s=\bar{n}_s} \right]^{-1}, \tag{32}$$

where $D(R_j) = \overline{(R_j - \bar{R}_j)^2}$ is variance of R_j. From (32), estimator can be obtained as

$$r \le \sigma_r C, \tag{33}$$

where $\sigma_r = \max_j \sqrt{D(R_j)}$,

$$C = \left[\sum_{j=1}^{N} \left(\frac{\partial f_j}{\partial n_s}\right)^2_{n_s=\bar{n}_s} \right]^{-0.5}. \tag{34}$$

For equidistant λ_j separated by interval $\Delta\lambda = (b-a)/(N-1)$ and sufficiently large N the sum in (34) can be represented as

$$\sum_{j=1}^{N} \left(\frac{\partial f_j}{\partial n_s}\right)^2_{n_s=\bar{n}_s} = N \left[\overline{\left(\frac{\partial f}{\partial n_s}\right)^2} + O(\Delta\lambda) \right],$$

where

$$\overline{\left(\frac{\partial f}{\partial n_s}\right)^2} = \frac{1}{b-a} \int_a^b \left(\frac{\partial f}{\partial n_s}\right)^2_{n_s=\bar{n}_s} d\lambda$$

represents the average value of function

$$\left(\frac{\partial f(\lambda, n_s)}{\partial n_s}\right)^2_{n_s=\bar{n}_s}$$

on interval $a \le \lambda \le b$. Then, $C \approx C'$where according to the law of large numbers

$$C' = \left[N \overline{\left(\frac{\partial f}{\partial n_s}\right)^2} \right]^{-0.5}. \tag{35}$$

In (33) σ_r characterizes the statistical properties of signals, and coefficient C is determined by the optical scheme of the refractometer. On this basis, calculation of C allows comparison of optical schemes of various refractometers from the viewpoint of their resolution capabilities. The coefficients C and C' for the studied refractometers are given in Table 2. They are calculated based on the relations

$$\frac{\partial f_j}{\partial n_s} = 2\mathrm{Re}\left[r_i^*(\lambda_j, n_s) \frac{\partial r_i(\lambda_j, n_s)}{\partial n_s} \right]$$

(i=p for p-polarized waves, i=s for s-polarized waves), (16), (21), (26) and (27). From the standpoint of conducting express measurements on the Photon RT[1] the following values were chosen

$$N = 15,\ \lambda_j = \lambda_1 + (j-1)\Delta\lambda,\ \Delta\lambda = 1\,\mathrm{nm}, \tag{36}$$

where $\lambda_1 = 793\,\mathrm{nm}$.

According to Table 2, an increase in refractometer sensitivity is accompanied by an improvement in its resolution, i.e., a decrease in C. This conclusion also applies to refractometers operating in the long-range plasmon mode scheme [1]. Indeed, the experimental dependencies $R(\lambda)$ shown in Fig. 4 of [1], corresponding to $\Delta n_s = 0$ (in this case $\lambda_{\min} = 812.8\,\mathrm{nm}$) and $\Delta n_s = 1.2 \cdot 10^{-4}$ under conditions (36), where $\lambda_1 = 805.8\,\mathrm{nm}$, correspond to $C = 5.59 \cdot 10^{-4}$, $C' = 5.73 \cdot 10^{-4}$. These values exceed by more than an order of magnitude the values C and C'listed in rows s_1 of Table 2. Table 2 also shows that despite the relatively small $N = 15$ approximation (35) is quite suitable for an order-of-magnitude estimation.

[1] https://www.essentoptics.com/rus/products/spectrophotometers/photon_rt/

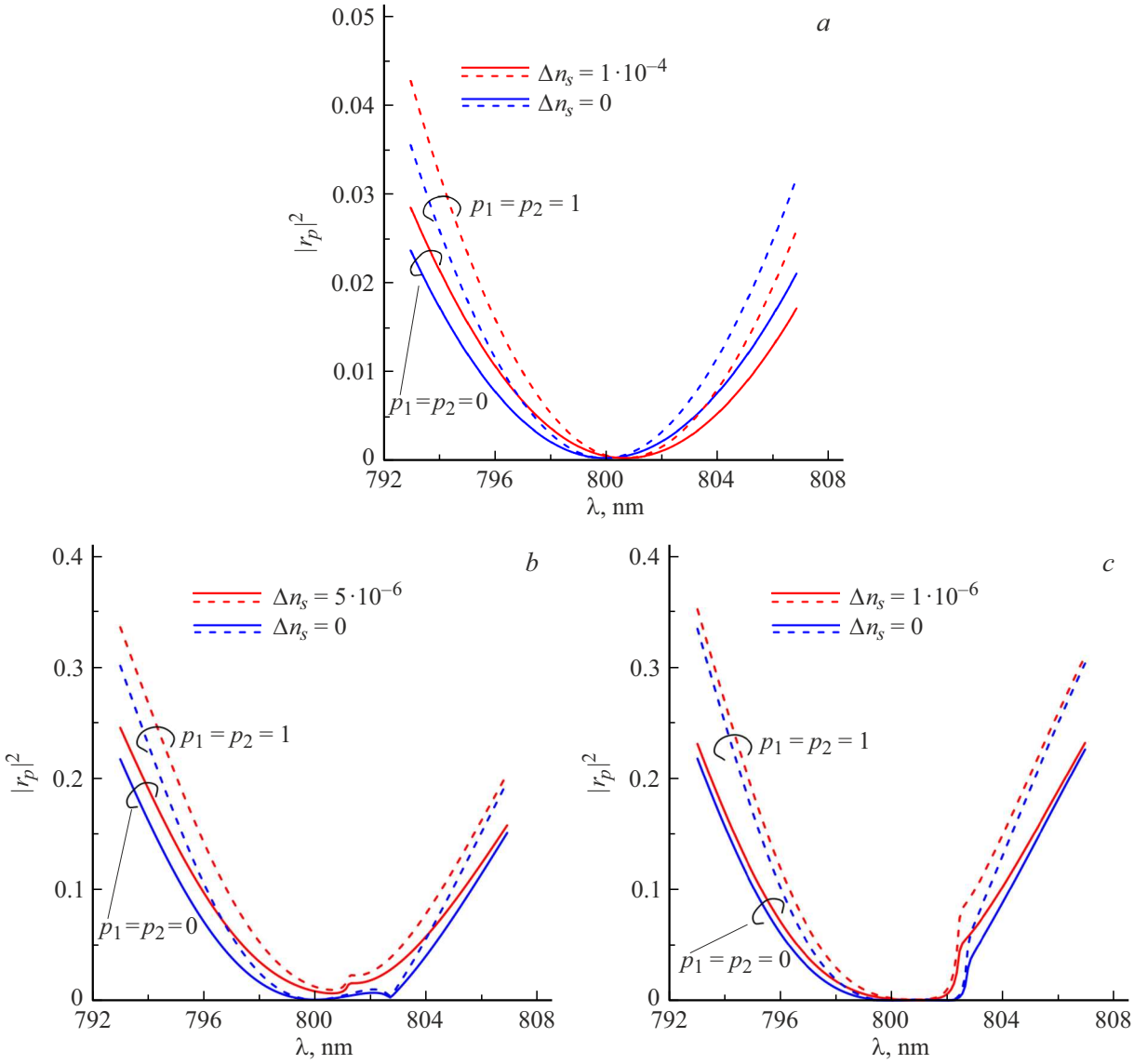

Figure 5. Modification of reflection spectra of refractometers with Kretschmann configuration (a) and optimized two-film refractometers using p- (b) and s- (c) polarized waves upon change in water refractive index by Δn_s.

5. Conclusion

A technique for calculating the sensitivity of spectroscopic refractometers with thin-film metal-dielectric structures based on a coupling prism has been developed. The reflection coefficient of refractometers is determined by multiplying characteristic matrices of films. Characteristic matrices of metallic films are calculated by numerically solving integral equations of the anomalous skin effect. Refractometers with the prism coupling structure–gold film–dielectric film–water with varying refractive index are studied in detail. Fused quartz is chosen as the material for the coupling prism and dielectric film. The dielectric permittivity of the gold ionic lattice and electron gas constants in the gold films are determined by processing literature data on spectral ellipsometry of partially transparent gold films. It is established that by optimal selection of metal and dielectric film thicknesses, two factors leading to the maximization of refractometer sensitivity zero light reflection from the coupling prism and excitation of a waveguide mode in the dielectric film under near-critical conditions can be combined. This allows raising the refractometer sensitivity up to $2.6 \cdot 10^5$ nm/RIU or $9.6 \cdot 10^5$ nm/RIU when using p- or s-polarized waves, respectively. The resolution capability of the refractometers is studied.

It is shown that the reflection spectra of well-studied plasmon mode refractometers and the proposed two-film refractometers differ qualitatively. On this basis, a criterion based on the least squares method is proposed for comparing the resolution capability of various thin-film metal-dielectric refractometers. Calculations show that an increase in refractometer sensitivity is accompanied

by an improvement in resolution capability. Among the considered devices, the maximum resolution belongs to two-film refractometers operating with *s*-polarized waves. There is a significant dependence of refractometer characteristics on the probabilities of specular electron reflection at gold film boundaries.

Funding

The work was carried out within the framework of the State Scientific Research Program of the Republic of Belarus „1.15 Photonics and Electronics for Innovation".

Conflict of interest

The authors declare no conflict of interest.

References

[1] R. Slavík, J. Homola. Sens. Actuators B: Chem., **123** (1), 10 (2007). DOI: 10.1016/j.snb.2006.08.020
[2] M. Piliarik, J. Homola. Opt. Express, **17** (19), 16505 (2009). DOI: 10.1364/oe.17.016505
[3] J.Y. Jing, Q. Wang, W.M. Zhao, B.T. Wang. Opt. Lasers Eng., **112**, 103 (2019). DOI: 10.1016/j.optlaseng.2018.09.013
[4] B. Hossain, A.K. Paul, M.A. Islam, M.F. Hossain, M.M. Rahman. Results in Optics, **7**, 100217 (2022). DOI: 10.1016/j.rio.2022.100217
[5] M. Myilsamy, P.C. Lordwin, A. Vibisha, S. Ponnan, J. Zbigniew, R.K. Balasundaram. Photonics Lett. Pol., **15** (2), 18 (2023). DOI: 10.4302/plp.v15i2.1206
[6] Q.M. Al-Bataineh, A.D. Telfah, C.J. Tavares, R. Hergenröder. Sens. Actuators A: Phys., **370**, 115266 (2024). DOI: 10.1016/j.sna.2024.115266
[7] F. Wang, Y. Wei, Y. Han. Sensors, **24** (15), 5050 (2024). DOI: 10.3390/s24155050
[8] D.V. Nesterenko, Z. Sekkat. Plasmonics, **8** (4), 1 (2013). DOI: 10.1007/s11468-013-9575-1
[9] A.B. Sotsky, M.M. Nazarov, S.S. Miheev, L.I. Sotskaya. Tech. Phys., **66**, 305 (2021). DOI: 10.1134/S1063784221020195.
[10] A.B. Sotsky, E.A. Chudakov, A.V. Shilov, L.I. Sotskaya. ZhTF, **94** (2), 267 (2024) (in Russian). DOI: 10.61011/JTF.2024.02.57082.185-23
[11] I.U. Primak. Tech. Phys., **49**, 1319 (2004). DOI: 10.1134/1.1809704.
[12] R.L. Olmon, B. Slovick, T.W. Johnson, D. Shelton, S.H. Oh, G.D. Boreman, M.B. Raschke. Phys. Rev. B, **86**, 235147 (2012). DOI: 10.1103/PhysRevB.86.235147
[13] E.T. Hu, Q.Y. Cai, R.J. Zhang, Y.F. Wei, W.C. Zhou, S.Y. Wang, Y.X. Zheng, W. Wei, L.Y. Chen. Opt. Lett., **41** (21), 4907 (2016). DOI: 10.1364/OL.41.004907
[14] D.I. Yakubovsky, A.V. Arsenin, Y.V. Stebunov, D.Y. Fedyanin, V.S. Volkov. Opt. Express, **25** (21), 25574 (2017). DOI: 10.1364/OE.25.025574
[15] A.V. Sokolov. *Opticheskiye svoistva metallov* (GIFML, M., 1961) (in Russian)
[16] A.B. Sotsky, E.A. Chudakov, L.I. Sotskaya. Opt. Spectrosc., **129**, 1023 (2021). DOI: 10.1134/S0030400X21070195.
[17] A.B. Sotsky, E.A. Chudakov, L.I. Sotskaya. JAS, **91**, 812 (2024). DOI: 10.1007/s10812-024-01789-7.
[18] *Handbook of Optical Constants of Solids,* ed. by E.D. Palik (Naval Research Laboratory, Washington, D.C., 1985). DOI: 10.1016/C2009-0-20920-2
[19] A.B. Sotsky. *Teoriya opticheskilh volnovodnykh elementov* (Mogilev State A. Kuleshov University, Mogilev, 2011) (in Russian)
[20] [*An Introduction to Optical Waveguides,* ed. by M.J. Adams (Wiley, N.Y., 1981).
[21] G.M. Hale, M.R. Querry. Appl. Opt., **12** (3), 555 (1973). DOI: 10.1364/ao.12.000555
[22] [*Mathematical handbook,* ed. by G.A. Korn, T.M. Korn (McGraw-Hill Book Company, N.Y., 1968)].
[23] G.G. Nenninger, M. Piliarik, J. Homola. Meas. Sci. Technol., **13** (12), 2038 (2002). DOI: 10.1088/0957-0233/13/12/332

Translated by J.Savelyeva